Proceedings of the 7th International Symposium on Cavitation
CAV2009 – Paper No. 72
August 17- 22, 2009, Ann Arbor, Michigan, USA

High speed motion in water with supercavitation for sub-, trans-, supersonic Mach numbers

V. V. Serebryakov
Institute of Hydromechanics
of NASU
8/4 Zheliabov Str., 0680 Kiev, Ukraine
serebryakov_vladimir@yahoo.com

I. N. Kirschner
Alion Science and Technology
Corporation,
RI 02842-6277, Newport, USA
IKirschner@AlionScience.com

G.H. Schnerr
Technische Universität
München
D-85748 Garching, Germany
schnerr@flm.mw.tu-muenchen.de

ABSTRACT
The results of research for supercavitating motion in water at very high speeds – comparable with sonic speed ~1500m/s – are presented. At such speeds the water is a compressible fluid and the basic compressible hydrodynamics of supercavitating flows together with practical approaches and experimental data are considered. The theory of ballistic projectiles motion is developed with emphasis on the problems of maximal range, lateral motion prediction and problems of minimal declination, hydro-elastic effects, and resonant oscillation frequencies. One main purpose of the article is an attempt to advance the level of understanding of the problem of very high-speed underwater launch by a comprehensive review of previous research on this topic.
Key words: supercavitation, super high speeds in water, compressibility, dynamics

INTRODUCTION
One of the most important applications of supercavitation is connected with the motion in water of small inertial projectiles of mass $\mathbf{M} \sim 0.1 - 0.5$ kg at very high speeds that are on the order of sonic speed in water, $a \sim 1450 : 1500$ m/s. For such speeds the motion occurs within a cavity that isolates most of the projectile surface from the ambient liquid in a process that gives the possibility of reaching very small drag coefficients. With this approach, small, non-propelled projectiles with very high initial speed can traverse considerable distances under water, distances comparable with distances that are similar to projectiles launched at a similar speed in air. Stable motion of such projectiles over relatively long distances has been repeatedly proved by experiments.
One of the most important problems here is maximization the range while conserving sufficient projectile kinetic energy at the end of the trajectory. This problem is especially closely connected with the problems of compressible flow in water. The flow processes are different for sub-, trans-, and supersonic speeds. Especially wave drag in the supersonic range is essential and causes considerable decrease of the cavity sizes and cavitation drag increase. Due to it achieved distances for supersonic speeds can be occurred considerable less as compared to the case of motion with subsonic speeds under the same initial conditions. Nevertheless this case conserves its importance for applications thank to considerable decreasing of time for overcoming given distance. This fact is important from the point of view of considerable increasing of speeds of modern high speed vehicles. One of the important problems is also the minimization of the deflection of the trajectory from a straight line due to initial perturbations during the launch process. This requires the development of a theory of projectile motion. The motion of a projectile in a cavity occurs in general along a curved trajectory, and at such high speeds, it causes very high lateral forces. Accordingly, hydro-elastic effects must be taken into account. The motion is of oscillatory nature that requires the consideration of the possibility of resonance processes. The problem as a whole is of complex nature and requires research in different directions. In this paper the attempt is made to improve the understanding of this problem as a whole and to develop practical approaches for estimating basic parameters which are necessary for the development of systems operating with very high-speed launch in water.

1. SHORT OVERVIEW
1.1 Experimental research
Due to the enormous high speeds, this research is complicated and expensive. However, it should be noted that a considerable subset of this research are of semi nature due to small enough projectile sizes that are convenient for further applications. One of the first experiments in this field is presented in reference [1]. The basic modern experimental research in this field started from subsonic experiments by Yu. Yakimov with his group [2-4] at the Institute of Mechanics of Moscow University, where around 1990 speeds up to ~ 1000 m/s were achieved. After that, very high subsonic speeds until ~ 1450 m/s were achieved at the Institute of Hydromechanics of NASU, Kiev, Ukraine [5-6]. Later, supersonic experiments at speeds with ~ 1600 m/s were performed at the Naval

Undersea Warfare Center Division, Newport, Rhode Island, in the United States [7]. The results of small scale subsonic experiments are presented in [8] and for very high ultrasonic speeds in [9]. These references reflect part of similar experiments only.

1.2 Theoretical research

Supercavitation is one of the complicated mathematical problem for flow with a priori unknown free boundaries. The basis of classic theory for incompressible fluid is presented by a number of well known publications [10-14]. Methods for nonlinear numerical computation of axisymmetric supercavitating flows in incompressible fluid are presented in particular by publications [15-17]. Nonlinear numerical computations with account of compressibility on the basic of isentropic compressible fluid approach are presented by publications [18-21], semi-numerical approach – [22]. More complicated model for hyper high speeds is used for computation in paper [23]. Very important is the case of slender cavities which provides the minimal cavitating drag. The problem here can be essentially simplified on the basis of slender body theory. Here on the base of Matched Asymptotic Expansion Method a linearized theory and effective practical approaches for prediction of axisymmetric supercavitation were developed [24-33]. Very important is the problem of cavitator penetration into water considerable part of the results in this field and references can be found in the book [34]. Specific gliding in the cavity problem was considered starting from known statement of blow of circle against circular free boundary [35] in number publications [36-38]. For the motion inside the cavity the interaction of the body stabilizing surfaces and devices is realized what is connected with consideration of 2 dimensions flows and other problems. Results related to this topic are presented by publications [39-42]. The problems of prediction of the motion inside the cavity were considered in publications [30-32, 43-44].

The problem of high-speed launch consideration as whole touches number of different fields with considerable volume information and especially in the field of compressible flows. So we try to outline the basics of the main approaches and to indicate the main physical ideas which are important from the point of view of further advancing theory and application of projectiles dynamics.

2. GOVERNING EQUATIONS OF FLOW

2.1 Simplest flow model

The basic idea to reach small drag coefficients for high-speed motion in water is to avoid the direct contact with the liquid by encapsulating the body in a vapor filled cavity. Creating a slender axisymmetric cavity can be explained with help of a simple model of radial flow, Fig. 1. In the case of prolate cavities the cavitator size is small and its drag is practically independent on the cavity form, additionally the cavity form is independent of the cavitator form which is defined by the cavitator drag only. The moving cavitator pushed the motionless fluid aside and its work is transformed into kinetic energy of mainly radial near cavity flow in the each motionless section which the cavitator has passed. In the main perturbed zone the main part of energy and impulse of flow is concentrated in finite region limited by the boundary $r = \psi(x,t)$ with extension of some more as compared to the semi-length of the cavitator and the cavity surface. This fact makes the cavity alike as a wake of finite type. Further the expansion of the cavity section together with the radial flow near the cavity is controlled by inertia and the pressure difference in the undisturbed flow and inside the cavity. In doing so the expansion process depends weakly on the surface $r = \psi(x,t)$ form (x, t – axial coordinate, time) and the less the more slender is surface of cavitator and cavity as whole. The cavity section reaches the maximal radius in the middle part and further starts to decrease by the action of the external pressure. In the back part of cavity unstable chaotic flow is realized where energy of radial flow is transformed into energy of the wake behind cavity. The least cavitating drag coefficient per cavity middle section C_D (the body close enough inserted in cavity) are reached for maximally slender cavities and the possibility of further decrease is limited by maximal aspect ratios of the bodies from the point of view of its strength.

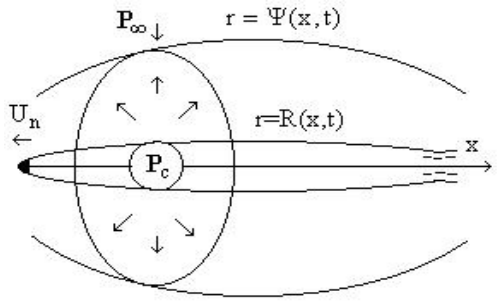

Figure 1: Radial flow model.

For real high speed of motion of supercavitating bodies in water values of $C_D \approx 0.05 : 0.001$ and less can be reached, for some cases the drag in water can be compared even with that in air. The basic parameter of cavitation flow is the cavitation number $\sigma = \Delta P / \left(\rho U_\infty^2 / 2\right)$, where ΔP - pressure difference between hydrostatic pressure in the flow and the pressure in cavity which is approximately zero for vapor cavities, ρ - density of water , U_∞ - speed of the undisturbed flow. The cavitation number σ in the case of a disk type cavitator defines the cavity aspect ratio λ which quickly increases if σ decreases. For very high speeds another basic parameter is the Mach number, $M_\infty = U_\infty / a_\infty$ where a_∞ - sonic speed in undisturbed flow. Flows with account for the compressibility are described by the same simplest model but with essential differences. In the case of incompressible flow we have essentially conservation of total kinetic and potential energy in each motionless section. But in compressible flow we have appearance of the wave drag of supersonic speeds especially of forward parts of the cavities and essential increase of the extension of the disturbed flow regime near cavities in the transonic range of Mach numbers.

2.2 Nonlinear approach

A typical nonlinear statement considers the cavitation problem in case of steady motion in an unbounded, ideal incompressible fluid with constant density ρ of the liquid. The Riabouchinsky closure (e.g., disk) scheme for the closure region of the cavity is usually used [15]. The cylindrical coordinate system (r, x) shown on figure 2 is used. The flow potential of perturbations φ satisfies the Laplace equation. For a given cavitator shape $r = r_1(x)$, the impenetrability condition on the cavitator is provided. The impenetrability condition and given pressure difference ΔP between the undisturbed flow and the cavity are assumed on the apriority unknown cavity shape $r = R(x)$. The perturbations at infinity tend to zero, the location of flow separation from the cavitator at $x = x_o$ is assumed to be fixed.

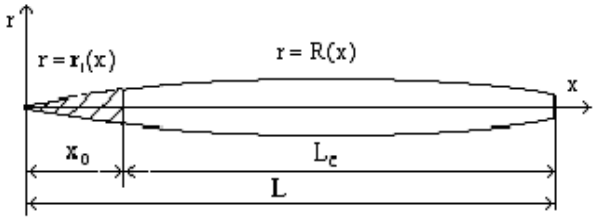

Figure. 2: Schematic of flow

In case of account for compressibility effects instead of the incompressible Laplace approach the potential flow model as known from gas dynamics including the equation for the sonic speed is used and is completed by an equation of state of water in the form of the Tait adiabatic curve Eq. (1):

$$\frac{P+B}{\rho^n} = \frac{P_\infty + B}{\rho_\infty^n}, \tag{1}$$

which gives the possibility to derive a compressible Bernoulli equation and the sonic speed of water:

$$\frac{n}{n-1}\frac{P+B}{\rho} + \frac{(U_\infty + u)^2 + v^2}{2} = \frac{n}{n-1}\frac{P_\infty + B}{\rho_\infty} + \frac{U_\infty^2}{2} \tag{2}$$

$$a^2 = \frac{dP}{d\rho} = \frac{n(P+B)}{\rho}, \tag{3}$$

where: $B \simeq 2985\,\text{bar}$, $n = 7.15$. The subscript ∞ indicates undisturbed free stream conditions at infinity. The quantities u and v are the axial and radial perturbation velocities along stream lines. For $M_\infty > 1$ shocks and their related losses have also to be taken into account.

2.3 Approximate approaches

In case of small disturbances the Prandtl-Glauert transformation of the Laplace equation is used. For $M_\infty < 1$ this is the acoustic equation for subsonic flow, for $M_\infty > 1$ this yields the wave equation for linearized supersonic flow.

$$\frac{\partial^2\varphi}{\partial r^2} + \frac{1}{r}\frac{\partial\varphi}{\partial r} + \left(1 - M_\infty^2\right)\frac{\partial^2\varphi}{\partial x^2} = 0 \tag{4}$$

On the basis of this equation the expansions of known slender body theory with accuracy of $(r^2 \ln 1/r^2, \delta^2 \ln 1/\delta^2)$ are received, δ - slenderness parameter. Using these expansions the equations for slender cavities are defined.

$M_\infty < 1$

$$\underbrace{\frac{1}{2R^2}\left(\frac{dR^2}{dx}\right)^2}_{(\ln 1/\delta^2)^{-1}} + \underbrace{\frac{d^2R^2}{dx^2}\ln\frac{m^2R^2}{4x(L-x)}}_{(1)} - \underbrace{\int_0^{x_o}\frac{\frac{d^2r_1^2}{dx^2}|_{x=x_1} - \frac{d^2R^2}{dx^2}}{|x_1 - x|}dx_1}_{(\ln 1/\delta^2)^{-1}} -$$

$$- \underbrace{\int_{x_o}^{L}\frac{\frac{d^2R^2}{dx^2}|_{x=x_1} - \frac{d^2R^2}{dx^2}}{|x_1 - x|}dx_1}_{(\ln 1/\delta^2)^{-1}} - \underbrace{\frac{\frac{dr_1^2}{dx}|_{x=0}}{x}}_{(\ln 1/\delta^2)^{-1}} + \underbrace{\frac{\frac{dR^2}{dx}|_{x=L}}{L-x}}_{(1)} = 2\sigma, \tag{5}$$

$M_\infty > 1$

$$\underbrace{\frac{1}{2R^2}\left(\frac{dR^2}{dx}\right)^2}_{(\ln 1/\delta)^{-1}} + \underbrace{\frac{d^2R^2}{dx^2}\ln\frac{m^2R^2}{4x^2}}_{(1)} - \underbrace{2\int_0^{x_0}\frac{\frac{d^2r_1^2}{dx^2}|_{x=x_1} - \frac{d^2R^2}{dx^2}}{|x_1 - x|}dx_1}_{(\ln 1/\delta)^{-1}} - .$$

$$- \underbrace{2\int_{x_0}^{x}\frac{\frac{d^2R^2}{dx^2}|_{x=x_1} - \frac{d^2R^2}{dx^2}}{|x_1 - x|}dx_1}_{(\ln 1/\delta)^{-1}} - \underbrace{2\frac{\frac{dr_1^2}{dx}|_{x=0}}{x}}_{(1)} = 2\sigma \tag{6}$$

In the case of slender cavities point closure is used where back closure action is modeled by source of pressure which is follow automatically on the base of Slender Body Theory expansions. For supersonic flow modeling we have not back response of flow to the its forward part and back closer is not required. Here $m^2 = |1 - M_\infty^2|$. In the case of transonic flow the small disturbances theory results in the following nonlinear equation for the potential:

$$\frac{\partial^2\varphi}{\partial r^2} + \frac{1}{r}\frac{\partial\varphi}{\partial r} + \left[\left(1 - M_\infty^2\right) - \frac{(n+1)M_\infty^2}{U_\infty}\frac{\partial\varphi}{\partial x}\right]\frac{\partial^2\varphi}{\partial x^2} = 0 \tag{7}$$

In case of flows of liquids the accuracy of Eq. (7) can be considerably less for the same cavity slenderness as compared to that of the equivalent equation for flows of gas/air. In addition the transonic range in water flows can be essentially wider as compared to that in air. The reason is the higher adiabatic coefficient in the equation of state for water.

3. PRACTICAL APPROACHES

Supercavitating flows are described by complicated equations. Further we present results and equations which were obtained in different ways including asymptotic expansions, slender body theory and by heuristic approaches. All equations are considered for the most interesting range of Mach numbers starting from incompressibility till $M_\infty \sim 2 : 2.5$. Most of these equations are verified by experimental and numerical data and are improved from point of view of more effective practical

use. Details of the derivation of these equations can be found in the publications of the list of references.

3.1 Estimation of cavitator drag

The practical dependence of the drag in steady incompressible flow for disk type cavitators (disk, blunted cone and i.e.) is :

$$D = c_d \pi R_n^2 \frac{\rho U_\infty^2}{2},\ c_d = c_{do}(1+\sigma),\ \text{disc: } c_{do} \approx 0.82 : 0.83, \quad (8)$$

R_n is the radius of the cavitator in the section of separation.

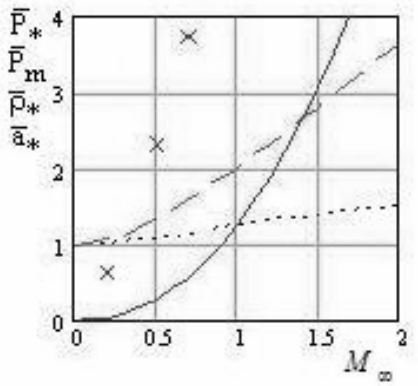

Figure 3: Values in stagnation zone for steady flow
——— - $\bar{P}_*$ pressure
× × × - $\bar{P}_m$ - impact pressure for disc penetration [18]
------- - $\bar{\rho}_*$ - mass density, – – – - $\bar{a}_*$ - sonic speed

The simplest approach for estimation of the drag with account for compressibility is on the basis of the equation for the pressure coefficient c_* at the stagnation point, also applicable in the transonic range, is:

$$c_* = \frac{2}{nM_\infty^2}\left[\left(1+\frac{n-1}{2}M_\infty^2\right)^{\frac{n}{(n-1)}} - 1\right], \quad (9)$$

$$M_\infty < 1 : c_d = 0.82 c_*(1+\sigma),\ M_\infty > 1 : \quad c_d = 0.82 c_* + \sigma$$

The influence of the compressibility near disk type cavitators is illustrated by values in the stagnation zone - pressure, density, sonic speed P_* (bar), $\rho_* = \bar{\rho}_* \rho_\infty$, $a_* = \bar{a}_* a_\infty$:

$$P_* = c_* \frac{\rho_\infty U_\infty^2}{2},\ \bar{\rho}_* = \left(1+\frac{n-1}{2}M_\infty^2\right)^{\frac{1}{(n-1)}},\ \bar{a}_*^2 = \left(1+\frac{n-1}{2}M_\infty^2\right), \quad (10)$$

Data for estimation of the values (10) are presented by Fig. 3 where $\bar{P}_* = P_* / 10^4 (\text{bar})$ the pressure impact values: $\bar{P}_m = P_m / 10^4$ for disc penetration in water is indicted on the basis of nonlinear numerical date [18]. The temperature in this range of M_∞ can be not above $\sim 100 - 200^o$ C, but in case of slender cavitators essential temperature increase is possible due to viscous flow.

For cones till semi-angles $2\gamma < 90^o$, $M_\infty < 0.8$, $\varepsilon = \tan\gamma$ the asymptotic approximation Eq. (11a) can be used. For slender cavitators, the lateral force can be estimated by the known equation (11b), applicable to a wide range of M_∞ where α is cavitator attack angle.

$$\text{a) } c_{do} = 2\varepsilon^2 \ln\frac{3}{2e}\frac{[1+(4/3)\varepsilon]}{m\varepsilon}\ ,\ \text{b) } F_\alpha = 2\alpha\pi R_n^2 \frac{\rho U_\infty^2}{2} \quad (11)$$

3.2 Simplest equations for the cavity form

Equations for steady slender axisymmetric cavity $r = R(x)$ are [24, 26]:

$$\mu \frac{d^2R^2}{dx^2} + \sigma = 0,\quad \left.\frac{dR^2}{dx}\right|_{x=0} = R_n\sqrt{\frac{2(c_d - k\sigma)}{k\mu}},\ \ R^2\big|_{x=0} = R_n^2. \quad (12)$$

For $\sigma = \text{const}$ the solution is an ellipsoidal cavity with known dependencies for the cavity maximal radius R_k, the cavity semi-length L_k, cavity aspect ratio $\lambda = L_k / R_k$ are:

$$R^2 = R_n^2 + R_n\sqrt{\frac{2(c_d - k\sigma)}{k\mu}}x - \frac{\sigma}{2\mu}x^2, \quad (13)$$

$$R_k = R_n\sqrt{\frac{c_d}{k\sigma}},\ \ \lambda = \sqrt{\frac{2\mu}{\sigma}},\ L_k = R_n\frac{\sqrt{2\mu c_d / k}}{\sigma} \quad (14)$$

Better accuracy for higher values of σ can be achieved by replacing $\mu_c = \mu c_d / (c_d - k\sigma)$ instead of μ.

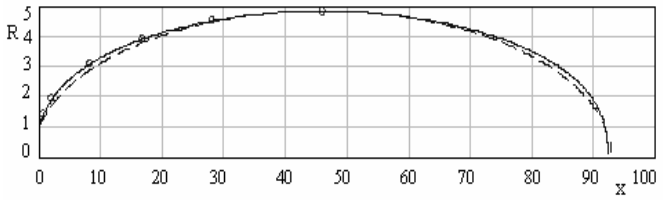

Figure 4: Cavity form behind disk incompressible fluid:
-- -- -- ellipsoidal cavity, $\sigma = 0.04$ Eq.(12),
∘∘∘∘ - nonlinear numerical data, $\sigma = 0.04$ [15].

The main idea of the resulting equation is as following: We use the first order outer solution for the most middle part of cavity surface, but in doing so we use two parameters in these equations on the base of more accurate approaches and in particular second order theory. Equations (12-14) include 2 typical values μ and k that have a clear physical meaning. The value μ characterizes the mass of the expanding cavity sections; the value k characterizes the axial transmission of energy along with the flow sections. Equations (12-14) are universal and applicable for estimation of the main part of the cavity in a wide range of M_∞ including subsonic, transonic, supersonic flow. But the values μ, k in these equations for

different ranges of M_∞ can be essentially different and given for further consideration. The accuracy of equations (12-14) as compared to nonlinear numerical data is demonstrated in Fig. 4 for prediction of steady, $\sigma = 0.04$ cavity. There are unsteady variants of these equations too.

These equations multiply verified by experiments and nonlinear numerical calculations and are one of the most hopeful approaches for practical estimation of axisymmetric cavities.

3.3 Incompressible fluid and subsonic flow for range of $M_\infty < 0.7 - 0.8$

The basis for practical dependencies for μ is a second order asymptotic solution for the aspect ratio λ and maximal radius R_k of slender axisymmetric cavity:

$$a)\ \sigma = \frac{2\ln\lambda / m\sqrt{e}}{\lambda^2},\quad b)\ R_k^2 = R_n^2\frac{c_d}{\sigma}\left[1 + 2\frac{\ln 2/\sqrt{e}}{\ln\lambda^2/m^2}\right]. \quad (15)$$

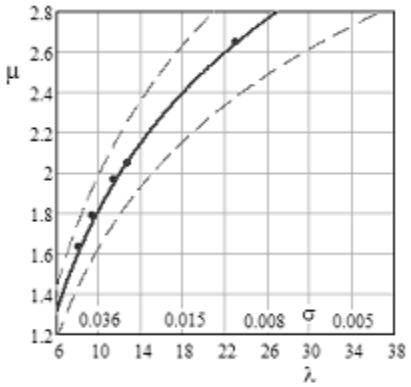

Figure 5: Dependence of inertial coefficient $\mu(\lambda)$, $\mu(\sigma)$
——— Eq. (16), -- -- -- values of 5% deflections for μ,
∘∘∘∘ - numerical calculations [15]

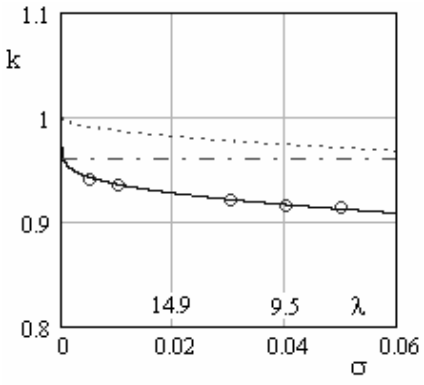

Figure 6: Dependence of $k = k(\sigma)$
on cavitation number for $M = 0$
——— Eq. (17), - - - - - H. Reichardt dependence,
∘∘∘∘ - numerical calculations [15]

For the range of $M_\infty < 0.7 : 0.8 :\ m^2 \sim 1 - M_\infty^2$. This solution defines a weak dependencies on λ and σ for values of μ, k :

$$\mu = \ln\frac{\lambda}{m\sqrt{e}} \simeq \ln\sqrt{\frac{\ln 2/m^2\sigma}{em^2\sigma}}\Bigg|_{\lambda\sim 8-15} \approx \ln\sqrt{\frac{1.5}{m^2\sigma}}, \quad (16)$$

$\sigma \sim 0.03 \div 0.01$: $\mu \sim 2 \div 2.3$,

$$k = k_\beta = 1 - \frac{2\ln 2/\sqrt{e}}{\ln m^2\lambda} \approx 1 - \frac{2\ln 2/\sqrt{e}}{\ln 4/m^2\sigma}, \quad (17)$$

$\sigma \sim 0.03 \div 0.01$: $k \sim 0.94 \div 1$

Calculation results of equations (16, 17) are illustrated in Figs. 5, 6. With account of Eq. (16) , the formula (15a) is transformed to the dependence :

$$\lambda^2 \simeq \frac{2}{\sigma}\ln\sqrt{\frac{\ln 2/m^2\sigma}{em^2\sigma}}\Bigg|_{\lambda=6-15} \approx \frac{\ln 1.5/\sigma}{\sigma} \quad (18)$$

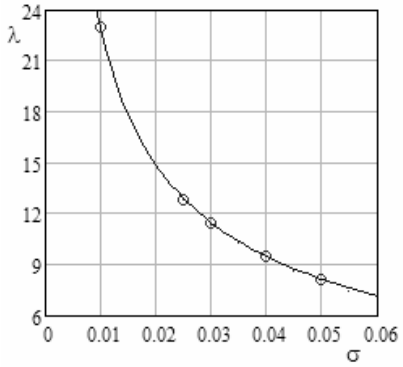

Figure 7: Dependence for cavity aspect ratio $\lambda = \lambda(\sigma)$
——— Eq.(18), ∘∘∘∘ numerical calculations [15].

Eq. (12, 14) are applicable for most of the middle part of the cavity. The forward cavity part near the disk is not described by this equation, as it can be seen from Fig. 4. The parabolic shape also not correctly describes cavity form at infinite where known M. Gurevich – N. Levinson asymptotic [12, 13] is:

$$R^2 = 2\sqrt{c_{do}}\frac{x}{\sqrt{\ln x}}\left[1 - \frac{1}{4}\frac{\ln\ln x}{\ln x} + \cdots\right] \sim \frac{x}{\ln x^{0.5}}. \quad (19)$$

More precisely, the approximate equation for the forward cavity part only applicable also just near disk type cavitator is:

$$R^2 = 1 + \frac{2\sqrt{(c_d - \sigma)}\,x}{\sqrt{\ln(1+\sqrt{e}x)/m^2}} - \frac{\sigma x^2}{\ln\left[(1+\sqrt{e}x)/m^2\right]} \quad (20)$$

In Eq. (19,20) all values are supposed to be dimensionless relay to disk type cavitator radius. For estimation of the forward part of the cavity only behind slender enough cones the first order asymptotic solution can be used, $\varepsilon = \tan\gamma$, γ - cone semi-angle, all values are supposed to be dimensionless relay to cavitator length $l = 1$:

$$R^2 = \left\{\varepsilon^2\left[2x\sqrt{\frac{\ln 1/m^2\varepsilon^2}{\ln x/m^2\varepsilon^2}} - 1\right] - \frac{\sigma(x-1)^2}{\ln x/m^2\varepsilon^2}\right\}, \quad (21)$$

An accurate enough asymptotic approximation for the cavity behind disk, $\sigma = \text{const}$ as a whole can be calculated by Eq. 22:

$$R^2 = R_n^2 + \frac{L_k^2}{\lambda_c^2}\sqrt{\frac{\mu_m}{\mu_{xx}}}\frac{x}{L_k}\left(2 - \frac{x}{L_k}\right),$$

$$\lambda_c^2 = \eta\lambda^2, \quad \eta = c_d/(c_d - k\sigma),$$

$$\mu_{xx} = 0.5\ln\left\{\frac{(x+\sqrt{e}\Delta)^2\left[\left(2+\sqrt{e}\frac{\Delta}{L_k}\right) - \frac{x}{L_k}\right]^2}{em^2\left[R_n^2 + \frac{L_k^2}{\lambda_c^2}\sqrt{\frac{\mu}{\mu_*}}\frac{x}{L_k}\left(2-\frac{x}{L_k}\right)\right]\left(1+\sqrt{e}\frac{\Delta}{L_k}\right)^4}\right\},$$

$$\mu_{xx}\big|_{x=L_k} = \mu_*, \text{ for : } \sigma \sim 0.01 \div 0.05 : \ \mu_* \sim 2 \qquad (22)$$

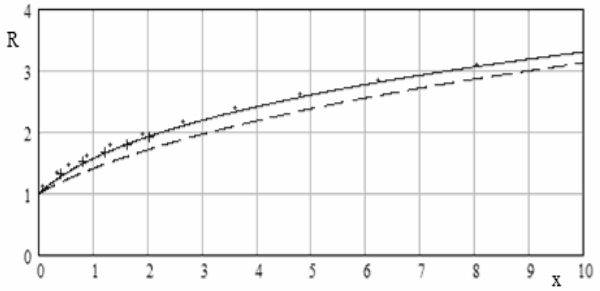

Figure 8: Nonlinear approximation of the cavity, $\sigma = 0.04$
– – – – ellipsoidal cavity form,
——— nonlinear approximation Eq. (22),
+ + + + G. Logvinovich (14) experimental data [14],
• • • • nonlinear numerical calculation [15].

Results based on equations (22) as compared to nonlinear numerical predictions for $M_\infty = 0$ are illustrated by Fig. 8.

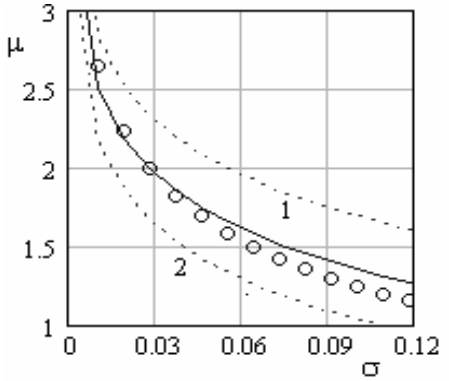

Figure 9: Compressibility influence on $\mu = \mu(\sigma, M)$

Incompressible fluid:
——— Eq. (16), ∘ ∘ ∘ ∘ numerical calculation [15].

Compressible fluid:
------- 1: Eq.(16), $M_\infty = 0.7$, ------- 2, Eq. (16), $M_\infty = 1.7$

3.4 Subsonic flow for $M_\infty < 0.7$ - 0.8

The equation for the aspect ratio in the range of supersonic speeds takes the same form as for subsonic flow (15b, 18). for $m^2 = |1 - M_\infty^2|$ and the same equation for μ value.

Fig. 9 illustrates action of compressibility on inertial coefficient μ and accordingly on cavity aspect ratio λ. But in the transonic range $M_\infty \sim 0.7 : 1.5$ the most important effect is the significant increase of the extension of the perturbation zone.

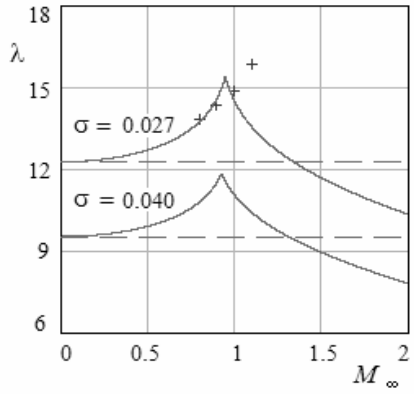

Figure 10: Aspect ratio in transonic flow
——— Eq, (18, 23), + + + numerical calculation [21].

For this range the dependence of m can be improved:

$$m^2 \sim \left[\left|1 - M^2\left(1 + \frac{n+1}{2}\sigma\right)\right| + \frac{n+1}{2}\sigma\right]\frac{1}{1+(n+1)\sigma/2} \qquad (23)$$

Fig. 10 demonstrates the estimation of the transonic cavity aspect ratio results based on equations (18, 23) as compared to the attempt by nonlinear calculations of [21]. Calculations were made for $\sigma = 0.0268$. Data of [21] are approximately recalculated for constant $\sigma = 0.0268$ on the basis of weakly changed values of $\lambda^2\sigma$.

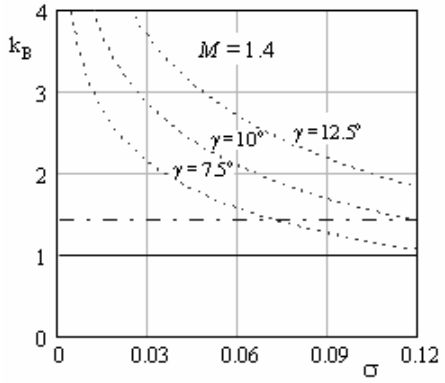

Figure 11: Dependence for $k = k_B(\sigma, \varepsilon)$, $M_\infty = 1.4$,
$\gamma = 7.5^o, 10^o, 12.5^o$
------- Eq. (25), –·–·– wave loss on the cone $\gamma \sim 10^o$

The situation with estimations of the supersonic cavity behind discs is not fully complete till now. Three terms of supersonic asymptotic at infinity for $M > 1$ with considerable differences as compared to subsonic asymptotic were found:

$$R^2 = \frac{K_S x}{(\ln x)^{3/2}}\left[1 - \frac{9}{4}\frac{\ln\ln x}{\ln x} + \frac{3}{2}\frac{\ln K_S m^2/4}{\ln x}\ldots\right] \sim \frac{x}{(\ln x)^{3/2}} \qquad (24)$$

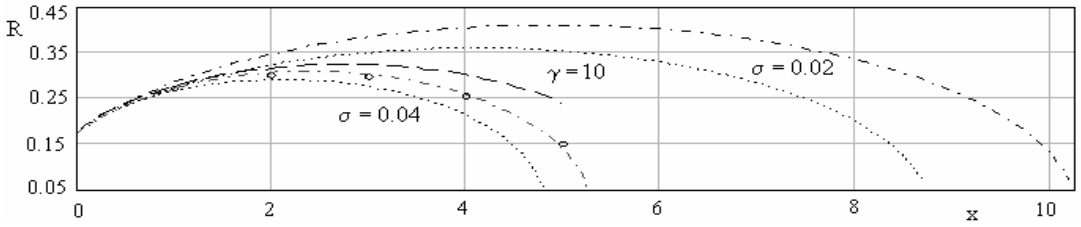

Figure 12: Compressibility influence on cavity form for cone $\gamma = 10^o$

∘ ∘ ∘ ∘ nonlinear numerical calculations $M_\infty = 0$, $\sigma = 0.04$ [16].

– – – – $M_\infty = 0$, $\sigma = 0.04$, $\sigma = 0.02$: Eq. (12-14, 16,17)

– – – – – calculations: $M_\infty < 1$: $M_\infty = 0.6$, $\sigma = 0.04$ - Eq. (12-14, 16, 17)

------- $M_\infty > 1$: calculations: $M_\infty = 1.5$, $\sigma = 0.04$, $\sigma = 0.02$ -Eq. (12-14, 16, 25)

and discovered considerable narrower forward part of a supersonic cavity as compared to subsonic one. Values of the asymptotic coefficient K_S where found for slender cavitators only [28]. Matching with outer for middle part of cavity solutions gives the possibility to find values of k for prediction of supersonic cavities behind slender cavitators [29]. In case of slender cones for $M_\infty > 1$ the value of $k = k_B$ was found and can be estimated by second order asymptotic dependence:

$$k = k_B = \frac{\ln\left(\frac{2e\lambda^2}{m^2}\right)}{\ln\left(\frac{2}{m^2\varepsilon^2}\right)} \approx \frac{\ln\left(\frac{2e\ln 1.5/m^2\sigma}{m^2\sigma}\right)}{\ln\left(\frac{2}{m^2\varepsilon^2}\right)}, \qquad (25)$$

where $\varepsilon = \tan\gamma$, γ-cone semi angle. The values of k_B dependent on the σ and on the cone semi-angle are demonstrated by Fig. 11 for $M_\infty = 1.4$ for a series of cone semi-angles: $\gamma = 7.5^o$, 10^o, 12.5^o. Using Eq. (16-17) for μ, k the supersonic cavity shape behind a slender cavitator can be easily estimated on the basis of simplest equations (12-14).

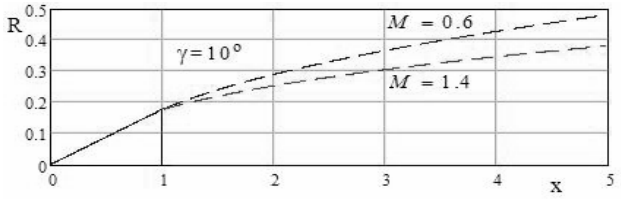

Figure 13: Cavity form for $\sigma = 0$ behind slender cone in sub- and supersonic flows

Fig. 12 illustrates calculated result for a supersonic cavity behind a slender cone as compared to subsonic flow and a cavity in incompressible flow for different cavitation numbers. The results for incompressible flow were verified by hopeful enough nonlinear numerical calculations [16].

The forward cavity part only behind slender cavitator can be estimated on the basis of first order asymptotic solutions:

$$R^2 = \left\{\varepsilon^2\left[2x\left(\frac{\ln(1/m^2\varepsilon^2)}{\ln(x/m^2\varepsilon^2)}\right)^{3/2} - 1\right] - \frac{\sigma(x-1)^2}{\ln(x/m^2\varepsilon^2)}\right\}_{x\to\infty} \to \frac{x}{(\ln x)^{3/2}} \quad (26)$$

Figure 13 illustrates results of calculations for forward parts of sub- and supersonic cavities behind a slender cone for $\sigma = 0$ based of Eq. (21, 26). These solutions were verified for $\sigma = 0$ by nonlinear numerical calculations [15, 16]. Figure 14 demonstrates calculation results for the forward part of the cavity behind disk for incompressible fluid as compared to subsonic, transonic and supersonic flow. For prediction of the cavity form second order asymptotic solution [29] is used where cavity semi-length is supposed as given. Figure 15 illustrates the supersonic cavity form behind small disc type cavitator as compared to ellipsoidal cavity.

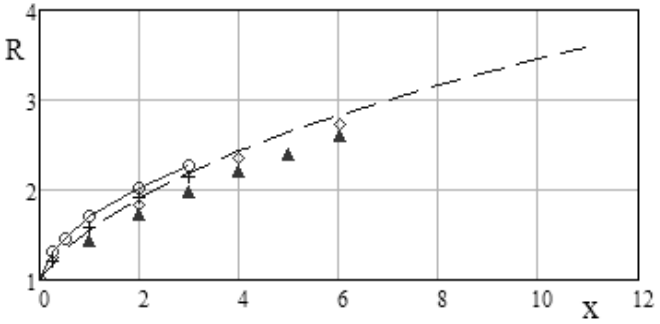

Figure 14: Forward part of cavity behind disk in compressible water

∘ ∘ ∘ ∘ $M_\infty = 0$ numerical calculation [15],

+ + + $M_\infty = 0$ experiment date [14]

– – – – $M_\infty = 0.6$ Eq. (20),

◊ ◊ ◊ ◊ $M_\infty = 1$, Δ Δ Δ Δ $M_\infty = 2$ numerical date [18-19]

3.5 Cavitating drag in compressible flows

The important difference of flows with $M_\infty > 0$ is the formation of wave drag on the cavitator and especially on the forward part of the cavities. The wave loss here can be very intense and is the higher the less cavitation number is. The appearance of wave drag leads to considerably higher

coefficients $k = k_B(\lambda, m)$ which are quickly increased for the cavity aspect ratios increasing.

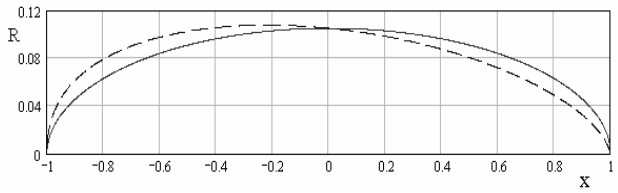

Figure 15: Comparison cavity form for $M_\infty > 0$ with ellipsoidal form

——— ellipsoidal cavity form

– – – cavity for $M_\infty \sim 1.4 > 0,\ \sigma \sim 0.04$

Significances of k values as distinguished with $M_\infty < 0$ where they are $k \sim 0.94 \div 1$, for $M_\infty > 0$ can reach the values $k_B \sim 2$, and more over what is illustrated by Fig. 11. As result supersonic cavities can have considerable smaller sizes as compared to subsonic ones, but with considerably higher cavitating drag coefficients. Below the equations for $k = k_\beta$, $k = k_B$ and also C_D and C_{D0} for forward cavity part for $M_\infty < 0$ and $M_\infty > 0$ in the case of cone are compared:

$$M_\infty < 1: \quad C_{D0} \sim \frac{1}{8}\frac{\ln \lambda / m\sqrt{e}}{\lambda^2}, \qquad k_\beta \sim 0.94 - 1$$

$$C_D \sim k_\beta \sigma = k_\beta 2\frac{\ln \lambda / m\sqrt{e}}{\lambda^2}. \qquad (27)$$

$$M_\infty > 1: C_{D0} \sim \frac{1}{8}\left(\frac{\ln 4\lambda / m}{\ln \sqrt{2} / m\varepsilon}\right)^2 \frac{\ln 4\lambda / m}{(\lambda)^2}, k_B = \left[\frac{\ln 2e\lambda^2/m^2}{\ln 2\sqrt{e}/m^2\varepsilon^2}\right]^2$$

$$C_D = k_B \sigma \sim \left(\frac{\ln 2e\lambda^2 / m^2}{\ln 2\sqrt{e} / m^2\varepsilon^2}\right)^2 \frac{2}{\lambda^2} \ln \frac{\lambda}{m\sqrt{e}} \qquad (28)$$

The expression for cavitating drag coefficient C_{DF} per the forward cavity section coincided with the body back section is:

$$D = C_{DF}\pi R_F^2 \rho U_\infty^2 / 2 = C_{VF} V_F^{2/3} \rho U_\infty^2 / 2$$

$$C_{DF} = \frac{k\mu}{8}\frac{\left(1 + 2\sigma\lambda_f^2 / \mu\right)^2}{\lambda_f^2}, \ C_{VF} = \sqrt[3]{\frac{\pi}{\kappa_p^2}}\frac{k\mu}{8}\frac{[1 + 2\lambda_f^2\sigma / \mu]^2}{(\lambda_f^2)^{4/3}} \qquad (29)$$

Like this the volume coefficient C_{VF} for motion of body of paraboloidal form is defined. Here λ_f - aspect ratio of the cavity part contained body per back sections of this part, R_F - radius of body back part which is touched the cavity, V_F - body volume. These expression are universal in general case for a wide range of M_∞ with different coefficients μ, k but based on an ellipsoidal cavity form which can be essentially different from real cavity for motion of small bodies in the forward part of very large cavities

3.6 Possibilities of compressibility account

The compressibility influence till $M_\infty \sim 0.6 : 0.7$ is not significant and here all calculations can be made on the basis of verified equations. Physically the zones of supersonic flow near surface of finite cavity are begun jet for subsonic speed of body motion. The flow near slender cavitators even under essentially supersonic speeds contains large zones of subsonic flow. For the range of $M_\infty \sim 0.6 \div 1$ and it would rather for not high supersonic speed of motion the values k can be not essentially different of 1 and can be estimated by Eq. (17). Values of μ with account of Eq. (23) can be calculated by equation (16). The estimation drag coefficient of disk type cavitators on the base of Eq. (9) is hopeful enough too. This fact gives the possibility to estimate the cavity form behind disks and slender cavitators for this range on the basis of Eq. (12-14) and more accurate including the zone near the disc type cavitator – Eqs (22). For transition into the range $M_\infty > 1$ the cavity very quickly is located in the supersonic zone. The theory in case of slender cavitators shows that the main part of the high wave losses establishes on the forward part of the cavities. As result even for slender cavitators the cavitating drag coefficients can be increased several times as compared to 1. With account of experimental verification of supersonic asymptotic of streamlines at infinity supersonic cavities behind slender cavitators can be estimated by equations (12-14) with account of dependence for k_B (25) and also by equation (26). The case of calculation behind disk for $M_\infty > 1$ causes higher complications and is not solved until now. The shock adiabatic curve for water is practically coinciding with the ordinary one and energy losses in the shock in water are not essential. Nevertheless it is need to expect jet more strong wave loss on the forward cavity part in case of the disk as compared to slender cavitators which can be appeared shortly enough for transition into range of $M_\infty > 1$.

4. EXPERIMENTAL RESEARCH

4.1 A typical launch process

The process of successful high-speed supercavitating projectile launch in water is realized in the following way. A projectile is launched into water at a speed of $\sim 1000 : 2000 \text{m/s}$ or even more. Usually a launch bubble of muzzle gas is created and a cavity considerably longer than the projectile develops.

The projectile travels along nearly straight line, and decelerates ballistically, so that the cavitation number increases and the cavity size decreases. At some point, the cavity boundary impinges on the projectile surface. Eventually most of the projectile surface becomes wetted, viscous drag causes very rapid deceleration and the trajectory is effectively terminated. Although a successful launch results in a nearly straight projectile trajectory, the projectile itself tends to oscillate within the cavity in pitch and yaw and is typically stabilized by a process referred to as “tail-slap,” wherein the after body grazes the cavity boundary.

Typical experiments have employed fairly small, slender, metal projectiles of mass on the order of $\mathbf{M} \sim 0.1 \div 0.5 \text{kg}$. The range is maximized by fabricating the projectiles from a heavy

material such as tungsten or steel, with a density $\rho \sim 7.8 \div 20\,\mathrm{g/cm^3}$. The projectile is designed to be closely conformal to the forward part of the cavity at the end of the trajectory, at which point the cavitation number is greatest, and the cavity dimensions are smallest. The cavitator size is selected such that the cavity nearly grazes the projectile surface at this moment. A disk-type cavitator is usually used, since it is associated with suitably stable projectile motion, and it is easily fabricated. However, it should be noted that, at very high speeds, such cavitators endure very high stresses that, even at steady speeds, can reach the yield limit of strongest steels. During water entry, under the conditions discussed in connection with Fig.3, the stresses are even greater.

Figure 16: Experimental launch scheme (not to scale).

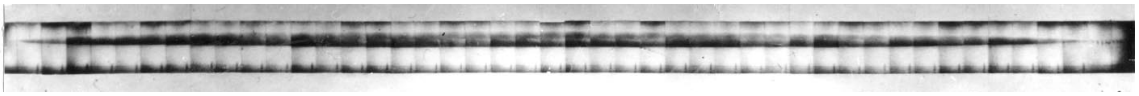

Figgure 17: Experimental cavity for $U \sim 1000\mathrm{m/s}$ behind disk with $R_n \sim 0.75\mathrm{mm}$, [5-6].

4.2 Experimental data

Most experimental data have been obtained at conditions near atmospheric pressure for motion in channels with free boundaries. In the following sections, the data involving the experiments described in references [5-7] are used. The projectile form and cavitator size are chosen on the basis of a cavity, the forward portion of which is close to a parabolic shape. Projectile stability is provided by sizing the cavitator such that the after body is wetted, or, alternatively by generating a slightly oversized cavity such that a tail-slap occurs. Typically, for very high-speed experiments at approximately atmospheric pressure with projectiles of small mass on the order of $\sim 0.1 \div 0.5\,\mathrm{kg}$, the cavities are very large. Under these conditions, for motion at a depth of $\sim 0.5\,\mathrm{m}$, the cavitation number is on the order of $\sigma \sim 2.1 \times 10^{-4}$. Ignoring the effects of facility boundaries and the free surface, the cavity length-to-cavitator radius ratio is on the order of $L_c / R_n \sim 29 \times 10^3$. Even for a cavitator as small as 1 mm, the associated cavity length is $L_c \sim 29\,\mathrm{m}$. In comparison, a steel projectile of mass $\mathbf{M} \sim 0.2\,\mathrm{kg}$ with an aspect ratio $\lambda_f \sim 10:15$ has a body length of only $L_b \sim 10:12\,\mathrm{cm}$. Even if the considerable blockage effect of the test facility is taken into account, the large cavity will allow for considerable motion of the small projectile within it. A rough schematic of the arrangement of the projectile within the cavity (not to scale) is presented in Fig 16. A high-speed composite image derived from sequential frames of a high-speed film of an experiment at a launch speed on the order of $\sim 1000\,\mathrm{m/s}$ is presented in figure 17 [5-6]. Experiments to ranges on the order of several scores of meters have been performed.

The main results of very high-speed supercavitating projectile experiments are as follows:

The practicality of stable motion over useful distances of small bodies enveloped in a supercavity has been demonstrated.

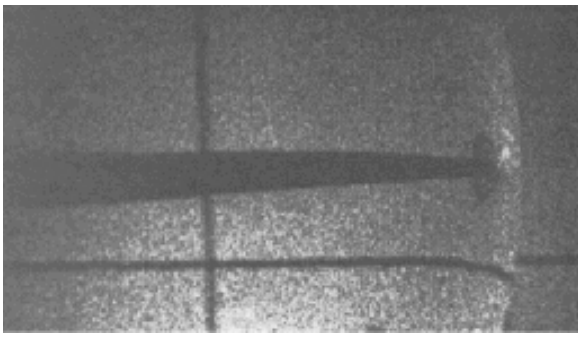

Figure 18: Supersonic cavity behind disk [7].

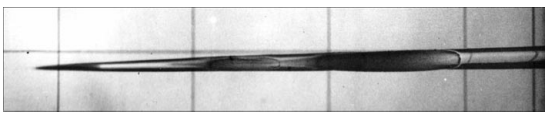

Figure 19: Demonstration of oscillating nature of the motion and projectile stabilization process, $M_\infty < 1$ [5-6]

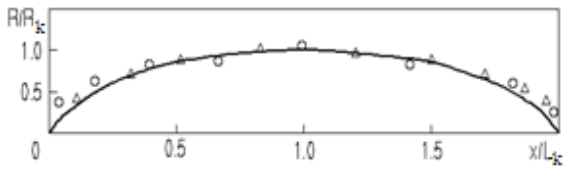

Figure 20: Ellipsoidal cavity form as compared to experimental cavities , points – experimental data for cavity form [5-6]

Very high sub- and supersonic speeds in water have been reached. See Figs. 17,19 [5-6] and 18 [7].

For range of speeds until $M_\infty \sim 2$ it was found that cavities have stable clear fixed surfaces. Theoretically and by experiments the oscillating nature of the projectiles motion and

possibility of resonance regimes for motion was discovered, see Figure 19.

Main problems of launch processes realization are connected firstly by the uncertainty of the quantity of successful lunching. As the estimation shows Fig. 3 the stresses on disk even for motion can exceed the yield point of strongest steels and considerably increased in the processes of initial blow of cavitators against water. Plastic deformation estimation shows that a steel disk cavitator under action of blow is deformed and becomes alike as a mushroom form. Additional lunching experiments may provide considerable more strong properties of metal under such specific of very short term blow processes.

This possibility can be verified by further experiments when we could catch projectiles which will not be destroyed for blow against obstacle. Other reason of unsuccessful launch can be too high initial perturbation of projectiles under launch which lead to high lateral forces and bended plastic deformations.

Lack of experiments is also impossibility to reach maximal distances with nature cavity closure at the end under 1 atm pressure so these distances are considerable over as compared to experimental treks. There are also considerable difficulties for the forward part of the cavity near the disk due to too high speed and especially thanks to essential change of optical properties of water under high pressure as it can be evident on figure 18. For 1 atm natural pressure and very high speeds the modeling of projectile motion in the cavity with the same as for projectile sizes is not possible too.

4.3 Verification of theoretical models

Experimental cavities are extreme slender like as needle ones. These cases are maximally suitable for approaches on the basis of slender body theory. At the same time nonlinear numerical modeling of alike cases is a very complicated problem which is not solved till now. The sizes of experimental cavities are usually considerable larger as comparison to distances to walls and channel free boundary. For estimation of the interference with boundaries in the range of $M_\infty < 0.6 \div 0.7$ we have dependencies [45]. However, for any case using experimental results for middle parts of cavities for verification of the theory is doubtful, due to considerable influence of boundaries. Especially essential boundaries influence for transonic flows and for this case and for $M_\infty > 1$ models to estimate boundaries interferences do not exist. This is the worse situation, due to the wide zone of perturbations. Here for motion near a free surface this zone action practically is neglected and considerable distortion are made also by the wall influence. The hopeful enough for all cases can be verification of the theory for forward part of cavities for distances of several projectile lengths in spite of problems for photo fixation of the cavity just form near disk type cavitators for too high speeds.

As a result of subsonic experiments they had proved closeness of very slender under very high speeds axisymmetric cavities to ellipsoidal form in spite of even considerable boundaries influence and also independence of expansion of the sections of this cavities what is demonstrated by Fig: 20, R_k, L_k - cavity maximal radius and length. Comparison of forward parts of cavities with known asymptotic of streamlines expansion at infinity by Gurevich- Levinson (19) [12,13] was made and confirmed this dependence. Data of supersonic experiments [7] give the possibility for verification of the asymptotic of stream line expansion at infinity in supersonic flow Eq. (24):

For verification the photo original of fragment figure 18 was used. Cavity form for weakly enough depend on M_∞ which was estimated on the basis of shock wave angle which is clear fixed on the photo. The experimental curves of the supersonic cavity form [7] were compared with subsonic asymptotic (19) with account found 3 terms and supersonic asymptotic (24) Fig. 21. For comparison booth theoretical curves are made as reciprocally intersected with experimental curve on the first figure at the section 3, on the second figure at the section 6. Experiments are corresponding to not very high supersonic Mach Numbers. The measurement of experimental radii was not as very accurate. On the photo it can be seen the range of the sections 4-6 the lateral blow of the projectile against cavity was occurred which what exited some increasing of the experimental cavity radiuses in for the next sections. Nevertheless, as it can be seen in Fig.21, the curve of the experimental cavity is situated considerable more close to supersonic asymptotic as distinguished to the subsonic one. These confirmations give essential assurance and can be regarded as a basis for validation of the equations developed on the basis of the Slender Body theory used under consideration.

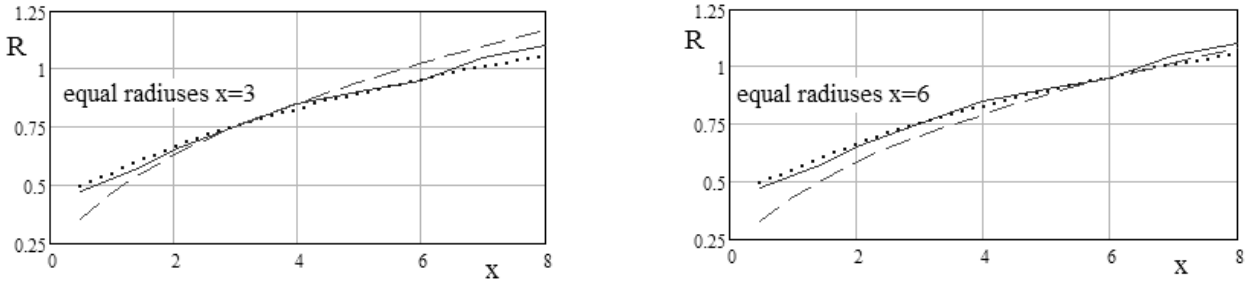

Figure 21: Verification of supersonic asymptotic of streamlines at infinity by experimental date [7]
——— experiment cavity form, - - - - - - - - supersonic asymptotic (24), – – – – subsonic asymptotic (19)

5. AXIAL AND LATERAL MOTION IN CAVITY

The theory of motion in cavity is described by complicated equations. There are here number of publication in particular [30,43,44] For small perturbed trajectories simple linearized and heuristic approaches can be used. The problems of axial and lateral motion can be considered separately

5.1 General equations of axial motion

For estimation of axial motion the cavitator drag only is taken into account. Due to extreme small values of cavitating drag coefficients a very low deceleration of the speed of motion under inertia is observed. This fact gives the possibility to use quasi steady approach for supercavitation modeling. The simplest model of axial body motion by inertia under drag which is proportional of to the speed square is described by:

$$\mathbf{M}\frac{dU}{dt}+\mathbf{K}U^2=0\ ,\quad U=\frac{dX}{dt}\ ,$$
$$\mathbf{K}=c_d\pi R_n^2\frac{\rho}{2}\ ,\quad U\big|_{t=0}=U_o\ ,\quad X\big|_{t=0}=0\ , \tag{30}$$

where $\mathbf{M}$, - body mass, $x=X(t)$ - trajectory length, $u=U(t)$ - body speed depend on time, $\mathbf{K}$ accounts for the cavitator drag. These equations can be easily transformed into the system with the simplest solution:

$$\frac{\mathbf{M}}{\mathbf{2}}\frac{dU^2}{dx}+\mathbf{K}U^2=0\ ,\ U\big|_{x=0}=U_o\ ,\ x=\frac{\mathbf{M}}{2\mathbf{K}}\ln\frac{U_o^2}{u^2} \tag{31}$$

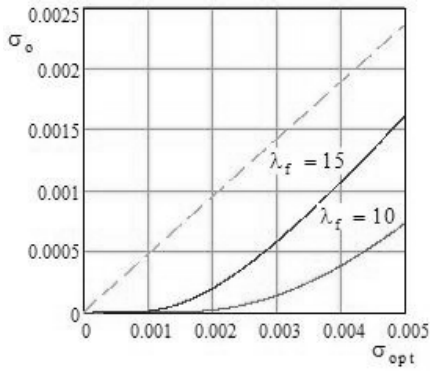

Figure 22: Optimal cavitation numbers
——— motion end in the forward cavity part paraboloid : Eq.(38) , – – – – motion end in the finite cavity: Eq. (39)

In general case it is supposed that the motion starts in the large cavity and finishes in smaller cavity when the back part of the projectile is connected with the cavity as it is shown in Fig. 16. The projectile with aspect ratio λ_f of near parabolic form we consider as given and inscribed in such cavity as we want with help coinciding given cavitator radius R_n. Trajectory length for motion in cavity until of reaching of the speed $u=U_c$ if motion speed until $U=U_c$ provides motion in cavity is defined on the basis of integral (31) by dependency:

$$X_c=\frac{M}{c_d\pi R_n^2\rho}\ln\frac{U_o^2}{U_c^2}=A\ln\frac{U_o^2}{U_c^2}\ , \tag{32}$$

5.2. Axial motion of a paraboloidal body in cavity

Firstly we consider the most general case when body can move for the final moment both at the forward cavity part of very large cavity Fig. 16 or in cavity with sizes what can be near to projectile sizes. In doing so the body has to be by form what would be close to the forward cavity part close to paraboloid. The cavitator size have to provide touch of back body with cavity for final moment. On the basis of equations for ellipsoidal cavity (14-16, 29) and equations (31, 32) the length of supercavitation part of trajectory is described by formula:

$$X=\frac{8}{9}\frac{1}{\sqrt[3]{\pi}}\frac{\rho_b}{\rho}\frac{\kappa_p^{2/3}}{k_c}\sqrt[3]{V}\frac{\sqrt[3]{\mu_c}}{\sigma_c^{4/3}}\frac{9\left(\frac{\lambda_f^2\sigma_c}{\mu_c}\right)^{4/3}}{\left[1+2\frac{\lambda_f^2\sigma_c}{\mu_c}\right]^2}\ln\frac{\sigma_c}{\sigma_o}=$$
$$=\frac{8}{9}\frac{1}{\sqrt[3]{\pi}}\frac{\rho_b}{\rho}\frac{\kappa_p^{2/3}}{k_c\mu_c}\sqrt[3]{V}\frac{9\left(\lambda_f^2\right)^{4/3}}{\left[1+2\frac{\lambda_f^2\sigma_c}{\mu_c}\right]^2}\ln\frac{\sigma_c}{\sigma_o} \tag{33}$$

This is an universal dependence, applicable both for incompressible and compressible flow in a wide range of M_∞ for coinciding significances of key coefficients $k=k_c$, $\mu=\mu_c$ corresponding their significances for cavity at the trajectory end. Here ρ_b, V - body mass density, volume, κ_f - show what part of volume of final cavity until back body section is filled by body, σ_o, σ_c - cavitation numbers for initial and final moments at the trajectory end. Optimization of dependence (33) for maximum of trajectory length X is made for λ_f, and σ_c. In result we have received two equations:

$$\text{a)}\ \frac{\lambda_f^2\sigma_c}{\mu_c}=1 \qquad \text{b)}\ \ln\frac{\sigma_c}{\sigma_o}=\frac{1+2\lambda_f^2/\mu_c}{4\lambda_f^2\sigma_c/\mu_c} \tag{34}$$

Optimization on λ_f only equation (34a) indicates that maximal distances are achieved for maximally filling by parabolic body the volume of final (ellipsoidal) cavity. The relation of the volumes of paraboloid form V_p close inscribed in ellipsoid cavity with volume V_e and relation of aspect ratios here for cavity and inscribed parabolic form are:

$$\kappa_{pe}=V_p/V_e=4/9\sim 0.445\ ,$$
$$\kappa_{pe}^{2/3}=(4/9)^{2/3}\sim 0.582\ ,\ \lambda_p=\lambda_c/\sqrt{2} \tag{35}$$

With account of Eq. (34a) the general dependence (33) is transformed into optimized dependence for maximal distances:

$$X_p=\frac{2}{\sqrt[3]{\pi}}\frac{4}{9}\frac{\rho_b}{\rho}\frac{\kappa_p^{2/3}}{k_c}\sqrt[3]{V}\frac{\sqrt[3]{\mu_c}}{\sigma_c^{4/3}}\ln\frac{\sigma_c}{\sigma_o} \tag{36}$$

By optimization for σ_c only equation (34b) indicates that the maximum of the trajectory length can be achieved for motion in the forward part cavity likely as in Fig. 16. The maximal

trajectory length is defined by the Eq. (33) and for a given body aspect ratio λ_f is defined by dependence:

$$X_f = \frac{8}{9}\frac{1}{\sqrt[3]{\pi}}\frac{\rho_b}{\rho}\frac{\kappa_p^{2/3}}{k_c}\sqrt[3]{V}\frac{\sqrt[3]{\mu_c}}{\sigma_c^{4/3}}\frac{9\left(\lambda_f^2\sigma_c/\mu_c\right)^{4/3}}{\left[1+2\lambda_f^2\sigma_c/\mu_c\right]^2}\ln\frac{\sigma_c}{\sigma_o}, \qquad (37)$$

where $\sigma_c = \sigma_{f\_opt}(\lambda_f, \sigma_o)$ is defined by Eq. (34b):

$$\ln\frac{\sigma_{f\_copt}}{\sigma_o} = \frac{1+2\lambda_f^2\sigma_{f\_opt}/\mu_c}{4\lambda_f^2\sigma_{f\_copt}/\mu_c} \qquad (38)$$

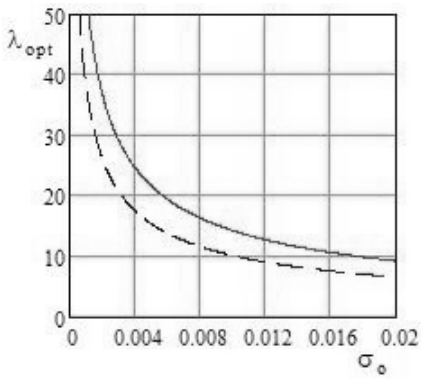

Figure 23: Body optimal aspect ratios depend on cavitation number σ_o
– – – – - close to paraboloidal form, Eq. (45)
——— - close to ellipsoidal form, Eq.(48)

5.3. Universal paraboloidal and ellipsoidal forms

If it would consider common optimization both on λ_f and σ_c the solution of the equations system (34a, 34b) give the condition which defines $\sigma_c = \sigma_{c\_opt}$ for both this cases too:

$$\ln\frac{\sigma_{c\_opt}}{\sigma_o} = \frac{3}{4}, \quad \sigma_{c\_opt} = \sigma_o e^{3/4} \sim 2.12\sigma_o \qquad (39)$$

Maximal distance on the base of Eq.(36), (39) is defined as:

$$X_{pm} = \frac{2}{3}\frac{1}{e\sqrt[3]{\pi}}\frac{\rho_b}{\rho}\frac{\kappa_p^{2/3}}{k_c}\sqrt[3]{V}\frac{\sqrt[3]{\mu_c}}{\sigma_o^{4/3}} \qquad (40)$$

Comparison of optimal cavitation numbers for motion end in the forward part of cavity and in closely inserted body in finite cavity is illustrated in Fig. 22.
The distance maximization under condition of maximal filling by the body of the cavity volume in the final moment is universal. This fact is valid both for bodies close to paraboloid and ellipsoidal form too! The dependence (35) for bodies of ellipsoid form the maximal distance is defined by the same as Eq. (36) Dependence, but with another coefficient:

$$X_e \approx \frac{2}{\sqrt[3]{\pi}}\sqrt[3]{\frac{4}{9}}\frac{\rho_b}{\rho}\frac{\kappa_p^{2/3}}{k_c}\sqrt[3]{V}\frac{\sqrt[3]{\mu_c}}{\sigma_c^{4/3}}\ln\frac{\sigma_c}{\sigma_o}. \qquad (41)$$

Like this as Eq.(40) the dependence for maximal distance of ellipsoid body is:

$$X_{em} \approx \sqrt[3]{\frac{3}{2}}\frac{1}{e\sqrt[3]{\pi}}\frac{\rho_b}{\rho}\kappa_p^{2/3}\sqrt[3]{V}\frac{\sqrt[3]{\mu_c}}{\sigma_o^{4/3}}. \qquad (42)$$

For the range of $M_\infty < 0.7 \div 08$, $\lambda_c \sim 10 \div 20$, $k_c \sim 0.94$ this main equations can be expressed accordingly. In the case of paraboloid form of the body:

$$X_p \approx 0.71\frac{\rho_b}{\rho}\kappa^{2/3}\sqrt[3]{V}\frac{\sqrt[3]{0.5\ln\frac{1.5}{m^2\sigma_c}}}{\sigma_c^{4/3}}\ln\frac{\sigma_c}{\sigma_o}, \qquad (43)$$

$$X_{pm} \approx 0.167\frac{\rho_b}{\rho}\kappa_p^{2/3}\sqrt[3]{V}\frac{\sqrt[3]{0.5\ln\frac{0.71}{m^2\sigma_c}}}{\sigma_o^{4/3}} \qquad (44)$$

Optimal body aspect ratio:

$$\lambda_{p\_opt} \sim 0.49\sqrt{\frac{\ln 0.71/m^2\sigma_o}{\sigma_o}}. \qquad (45)$$

In the case of near ellipsoid form of body:

$$X_e \sim 1.1\frac{\rho_b}{\rho}\kappa^{2/3}\sqrt[3]{V}\frac{\sqrt[3]{0.5\ln\frac{1.5}{m^2\sigma_c}}}{\sigma_c^{4/3}}\ln\frac{\sigma_c}{\sigma_o}, \qquad (46)$$

$$X_{em} = 0.288\frac{\rho_b}{\rho}\kappa_p^{2/3}\sqrt[3]{V}\frac{\sqrt[3]{0.5\ln\frac{0.71}{m^2\sigma_c}}}{\sigma_o^{4/3}}. \qquad (47)$$

The optimal body aspect ratio is:

$$\lambda_{e\_opt} \sim 0.69\sqrt{\frac{\ln 0.71/m^2\sigma_o}{\sigma_o}} \qquad (48)$$

Comparison of optimal cavitation numbers which realize maximal distances for end of motion in the case of closely inserted in finite cavity paraboloidal and ellipsoidal bodies forms is illustrated by Fig. 23.

5.4 Maximizing projectile range

Given and not changed are values of ρ and of the gravity field pressure ΔP. The range of change ρ_b/ρ is also limited by values $\sim 8 \div 15$. From the point of view of effective launch most important is to reach a given distances and in doing so to miss till final moment small enough part of initial projectile energy what is required for impact on the obstacle. With account limitation of reasonable initial launch values of speed the most important possibility of the launch systems efficiency is the possibility of maximal increasing of the reaching distances under given initial speed. This problem can be reformulated as equaling the possibility of receiving a given distance by minimization of the initial speed, too.
There are two possibilities to reach a maximal distance under the process optimization. For the paraboloidal body form this means optimization on the cavitation number at the final moment under given body aspect ratio Maximal range here is

defined by equation (37, 38). The cavitator size here is designed for inscribing paraboloidal body in the forward part of cavity with cavitation number defined by Eq. (38) depending on initial cavitation number. In the second way the one parameter optimization is possible both for parabolic and elliptic body forms the maximal distance is reached in the case when body maximally closely fills the final finite cavity.

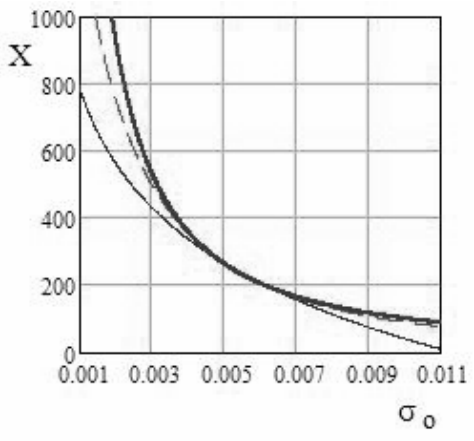

Figure 24: Maximal ranges – paraboloidal form
━━━━ Eq. (44), ——— Eq. (43) for $\lambda = 15$
– – – – – Equations (37-38) for $\lambda = 15$

The maximal distance here is defined by equations (36, 41) with account of sizes for cavitator which provide close inscribing of the body in final given finite cavity. For both cases of optimization we have to chose the points with characteristic pressures and make optimization for this points so in reality we have hydrostatic pressure changing. Under these conditions our design for typical points of pressure under condition of constant initial speed of pressure will be optimal only for these values of pressure only. For another pressures changing along depth this design will not be optimal and can be near optimal only. For both cases under fixation of ΔP and ρ_b / ρ we have the structure of dependence for length of cavitating part of trajectory (49a) which physically expresses the dependence (49b) :

$$\text{a) } X \sim X(V, \sigma_c, \sigma_o) \qquad \text{b) } X \sim X(M, U_c, U_o) \qquad (49)$$

Under given mass **M** and value defined body energy at the final moment U_c the trajectory length can be any long under infinite increasing of initial speed U_o. With account of given characteristic maximal pressure ΔP_m given distance length X, initial speed U_o and energy at the given trajectory end U_c definite defines value of body mass **M** : $\mathbf{M} = M(X, U_c, U_o)$
For further using with account of changing of pressure for given values **M**, U_c, U_o the length of distance will be coincide for given point $\Delta P = \Delta P_m$ however it will be more long for less pressures and more short for more high pressures.

The values U_c at the end of given trajectory length for $\Delta P = \Delta P_m$ will be the same under more small pressures. Under conditions when we have the possibility to change the initial speed two optimization parameters give the possibility to optimize also parameter of the body form (body aspect ratio λ) from point of view of reaching of maximal distance. Optimal aspect ratios λ are realized depending on σ_o : equations (39, 45, 48) and under considerable increasing of initial speeds can not be over of definite values of λ from point of view body strength. Chosen maximal possible aspect ratio of projectile from point of strength as $\lambda_{kr} \sim 15$ critical values of initial cavitation numbers for parabolic σ_{kr_p} and ellipsoid σ_{kr_e} forms are estimated by equations (50, 51).

$$\sigma_{kr\_p} = e^{-3/4} \left. \frac{\ln(\lambda_{kr}\sqrt{2} / m\sqrt{e})}{\lambda_{kr}^2} \right|_{\lambda\sim 15,\ m\sim 1} \sim 0.0054 , \qquad (50)$$

$$\sigma_{kr\_e} = e^{-3/4} \left. \frac{2\ln(\lambda_{kr} / m\sqrt{e})}{\lambda_{kr}^2} \right|_{\lambda\sim 15,\ m\sim 1} \sim 0.0093 . \qquad (51)$$

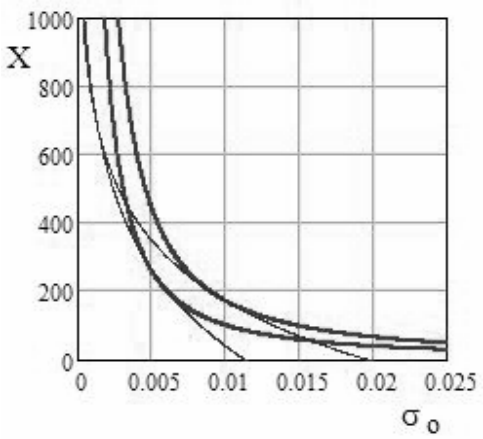

Figure 25: Maximal ranges comparison paraboloid–ellipsoid forms, (for paraboloid curves are below ellipsoid ones)
━━━━ Eq. (44, 47), ——— Eq (43, 46) for $\lambda = 15$

These cavitation numbers divide range of pressures (depths) on two parts. The part of more high pressures is when optimization is realized for body closely inserted in the cavity at the trajectory end. The part of the less pressure is where optimization is realized for motion of the body at final moment in the forward part of cavity. Body aspect ratio optimization equation (50, 51) is occurred as possible for the ranges of $\sigma_{op} > 0.0054$, $\sigma_{oe} > 0.0093$. Under less initial cavitation numbers and given maximal body aspect ratios $\lambda_f \sim 15$ considerable better to use optimization for motion in the forward part of cavity where maximal distance is defined by equation (37,38). In doing so the cavitator size is designed under condition of inscribing of body in the forward part of cavity under given characteristic maximal pressure $\Delta P = \Delta P_m$. For less and more high pressures calculation is made on the general equation (33) under value of σ_c defined for $\Delta P = \Delta P_m$. Critical values are different due to the parabolic projectile form have less volume as compared too ellipsoidal form for inscribing in the finite cavity at the final moment. Due to it

parabolic form projectiles have less critical depth and accordingly cavitation number.

Figs, 24 and 25 illustrate the comparison of calculated results for maximal ranges under $k \sim 1$ $m \sim 1$, $\kappa = 1$, $\rho_b / \rho = 1$, $V = 1$ and different ways of optimization under equal body aspect ratios and masses. In Fig: 25 the over curves correspond to ellipsoidal form, below – paraboloidal body form. On Figs 24, 25 touching points correspond to critical values of initial cavitation numbers (50, 51). In this point for $U_o \sim 1500 m/s$ bodies by mass $0.3kg$ have reached distance length $\sim 100m$ in the case of parabolic form under $\Delta P \sim 60bar$, ellipsoidal form under $\Delta P \sim 100bar$. Since smaller cavitation numbers trajectory length become practically as equal for paraboloidal and ellipsoidal forms with account that paraboloidal form is inscribed in cavity under smaller cavitation numbers for the same body aspect ratios.

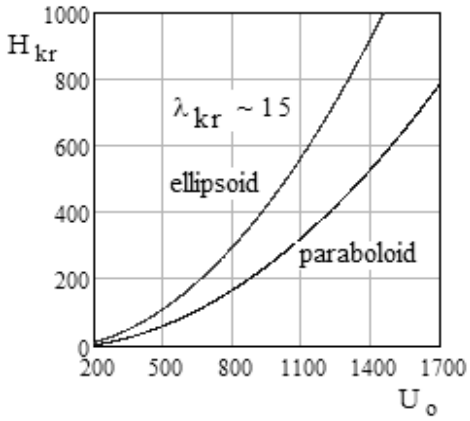

Figure 26: Critical depths H_{kr} (m) depend on initial speed U_o (m/s)

——— paraboloid form Eq. (50)

– – – – – ellipsoidal form Eq. (51)

Figure (26) illustrates critical lines of pressure depend on initial projectile speed in the case of paraboloidal and ellipsoidal forms It should be noted that the ellipsoidal body form under the same conditions give the possibility to reach longer distances under high pressures but have essential lack with respect to required additional stabilizer devises and is not good applicable for small pressures. The parabolic form is considerably more universal giving some less long distances for high pressures but it is applicable and for small pressures too, giving the possibility to reach maximal distances under given body aspect ratios. For case of paraboloid form there is possibility in particular of an automatic stabilization with the help of multiple touching by body back part of the cavity under angular oscillations of the projectiles.

5.5 Other constraints

Launch optimization process under given trajectory length and energy at the trajectory length give not the possibility to account additional conditions and limitations if we have no some reserves of values of initial speeds and distances. When we have these reserves they can be used to account for additional conditions. In particular if we have limitation on projectile energy for final moment $E_c = \rho_b V U_c^2 / 2$ which can not be less as a required value we can optimize mass (volume V) of projectile from point of view maximization of trajectory length under this condition on the basis of equation (36, 41). The optimal values of V here are defined by dependence (52a) and corresponds to the dependence (52b) for cavitation number σ_o and energies of projectiles for initial and final moments:

$$a)\quad V = e\sigma_o \frac{\rho}{\rho_b}\frac{E_c}{\Delta P}\quad ,\quad b)\ \sigma_c = e\sigma_o,\ E_c = E_o / e \tag{52}$$

These dependencies are not essentially different as compared to conditions of main optimization (39). For limitations of the projectile energy at the final moment maximal distance will be reached under some more high initial speeds. Under limitation of the energy of launch device optimal V is defined by (52b) what corresponds to equations for the cavitation numbers and energies for the initial and final moments (53b):

$$a)\quad V = e\sigma_o \frac{\rho}{\rho_b}\frac{E_c}{\Delta P},\quad b)\ \sigma_c = e^3\sigma_o,\ E_c = E_o / e^3 \tag{53}$$

Conditions for given initial energy were considered also in [43] and after that in [46]. Conditions for minimal initial energy and momentum of the projectile under given range and body λ_f can be found too for both cases of cavitational trajectory end. This condition defines optimal value (54) of projectile volume V_{opt}, where $B(\lambda)$ is defined by dependence (55):

$$V_{opt} = \left(\frac{X_c}{3(\lambda^2)^{4/3} B(\lambda)}\right)^3 \tag{54}$$

$$B(\lambda) = X_c / \sqrt[3]{V}\,(\lambda^2)^{4/3} \ln\frac{\sigma_c}{\sigma_o} \tag{55}$$

Figure 27 illustrates values of optimal volumes in $(cm)^3$ - Eq.(55) for paraboloid form depend on body aspect ratio λ under give trajectory range $X_c \sim 100m$ in the case of close inserting body in finite cavity at the trajectory end - Eq. 36. Two cases of the body mass densities are used, $\kappa \sim 1$, $k_c \sim 0.93$.

It is important to note that for limitation of the initial energy of projectile maximal distances will be reached for considerable more high initial speeds and less projectile volumes but under considerable decrease of the energy at the trajectory end. It is possible to account of other limitations, important from the point of view increasing of efficiency of very high-speed launch systems in water too. It is interesting also possibility of estimation reached distances and their optimization with account motion under angle relay to gravity field. Trajectory length can be expressed by dependence:

$$X = A \ln \sigma_c / \sigma_o, \tag{56}$$

where A is defined by parameters of end cavity and is not changed along motion. For motion in hydrostatic pressure field with account of gravity dependence for trajectory length under given σ_c, (λ_c) is defined by equation:

$$X = \mathbf{A} \ln \frac{\sigma_c \rho U_o^2 / 2}{\Delta P_o + \gamma X_c \cos\eta} \qquad (57)$$

where $\gamma = \rho g$ weight density of fluid, η is calculated from gravity direction against clock rotation. Aspect ratio optimization here is made analogously constant pressure but for this case for given trajectory length and after that minimization initial speed. In doing so cavitation numbers are considered for pressure values at the trajectory end.

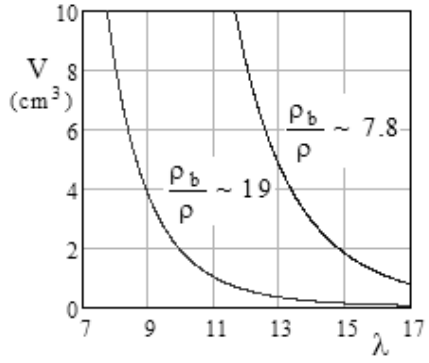

Figure 27: Dependence for optimal volumes depend on body aspect ratio under given range Eq. 55. Motion of paraboloidal body closely inserted in cavity at trajectory end.

Relations of optimal cavitation number (39) are occurred the same as for motion along trajectory under constant pressure. For motion along direction to free surfaces the bodies can flight out from water due to the cavity will not be closed. Condition of body free flight out from water for $\gamma \cos\eta < 0$ is:

$$\sigma_o \le \frac{\sigma_c}{1 + \left(1 + \dfrac{\mathbf{A}\gamma\cos\eta}{\Delta P_o}\right)} e^{-[1+(\mathbf{A}\gamma\cos\eta)/\Delta P_O]} \qquad \gamma\cos\eta < 0 \qquad (58)$$

Here ΔP_o - defines given pressure for initial moment.

5.6 Accounting for compressibility

Key moments of compressibility account can be made clearly on the basis of general equations (37,38) and (36, 41) passing coefficients values μ, k which defines the compressibility influence on the trajectory length. Here it is an important fact that the trajectory length is defined by cavity at the trajectory end defined projectile drag coefficient. Under supersonic speed at the final moment this coefficient can occur as it clear on Fig.11 in several times more over as compared motion for subsonic speeds. With account optimal relation initial and end speeds $U_o \sim 2.1 U_c$ increasing initial speed till values $U_o \sim 3000 \div 3200 \text{m/s}$ for sonic speed in water $a \sim 1500 \text{m/s}$ will lead to increase of maximal trajectory lengths. But here it can be possible to have the problems with motion in essentially smaller supersonic cavity. Further initial speed increasing can be by negative action decreasing the trajectory length. Nevertheless using of supersonic lunch is important thank to it can considerable decrease time of projectile run along given range. But it is need account that in the case of supersonic lunch for decreasing of speed along trajectory until sonic speed created under body penetration into water wave chock can go after projectile and close the cavity. The trajectory end for $M_\infty < 1$ in transonic range can increase the trajectory length due to larger aspect ratio of the cavities in this range.

6. LATERAL MOTION

6.1 Some peculiarities of the motion

Convenient approach is the application of equality conditions of all inner forces and moments projected to normal and tangential axes of the motion trajectory $y = y(x)$. In the case of level motion, the system of equations for the trajectory is:

$$\mathbf{M}U_s \frac{d\theta}{dt} - F_n + \mathbf{M}g\cos\theta = 0, \quad \frac{dy}{dx} = \tan\theta,$$
$$\mathbf{J}\frac{d^2(\theta+\alpha)}{dt^2} + \mathcal{M} = 0. \qquad (59)$$

Here $\mathbf{M}$ is the body mass, $\mathbf{J}$ is the longitudinal moment of inertia, t is the time, $U_s(t)$ is the velocity component along the trajectory defined by the addition to equation (59), α, θ are the angle of attack and the angle tangential to the trajectory, respectively. Equations (59) are written in with F_n as the normal component and $\mathcal{M}$ as the moment of the sums of all inner forces acting on the body, including hydrodynamics forces. In general, the process of motion can be imagined as follows. A moving cavitator creates a cavity surface and after that, the body moves on this surface. The trajectory of the cavitator and the trajectory of all parts or the body interacting by hydrodynamic way with the cavity (planning, stabilization, etc.) do not coincide with the trajectory of the center of mass. The body rotates, oscillates, and bends, and, as a result, the local speeds and angles of attack of it different components that interact with the cavity are significantly different. The cavitator in this system essentially marks the curved trajectory of the centers of expanding cavity sections. In doing so, the cavitator imparts to the sections a definite lateral speed and inertial impulse and after that, the sections and body components interact with finite time lag. Besides, a cavity for motion can be deformed under different external factors, some of the most significant being lateral gravity influence and gas injection, and even for motion of a rigid body in an empty cavity connected with the possibility of appearance of power oscillation processes. Thus, we have a complicated complex process including rigid and hydro-elastic body oscillations under the action of cavity deformations and waves on its surface which can appear for motion.

6.2 Fluid-body interaction effects

The key problem is calculation of planeing on the cavity surface. Planeing theory started from known publications by E Paryshev [35] for planning cylinder on cylindrical free surface and after that was developed through many investigations [36-38]. Essential to this problem is the application of the strip model for the hydrodynamic interaction with the cavity. In considerable part cases the linear presentation of the lateral force depend on attack angle can be used as based on the added

mass m at the body end part coincided with separation section. Given a sufficiently wetted back part of the body, known linear theory for slender body lift (11b) here can be applicable. It is important for some cases can be account for compressibility for planning for at sub-, trans-, supersonic speeds too.

6.3 Hydro-elastic effects

The model problem based on differential equations for an elastic beam is:

$$\text{a)}\quad \frac{\partial^2}{\partial x^2}\left[\mathrm{Ei}(x)\frac{\partial^2 y}{\partial x^2}\right]+\mathrm{M}(x)\frac{\partial^2 y}{\partial t^2}=0,$$

$$\text{b)}\quad \left[\mathrm{Ei}(x)\frac{\partial^3 y}{\partial x^3}-mU_s^2\frac{\partial y}{\partial x}\right]\Bigg|_{x=-a}=0,\ \left.\frac{\partial^3 y}{\partial x^3}\right|_{x=a_1}=0, \qquad (60)$$

$$\text{c)}\quad \left.\frac{\partial^2 y}{\partial x^2}\right|_{x=-a}=0,\ \left.\frac{\partial^2 y}{\partial x^2}\right|_{x=a_1}=0.$$

Here, $i(x)=i_*\bar{i}(x)$ is the linear moment of inertia and $\mathrm{M}(x)=\mathrm{M}_*\bar{\mathrm{M}}(x)$ is the mass of beam sections. E is the elastic modulus. The center of mass is located at the coordinate, $x=0$. Distances a and a_1 are measured from the center of mass to the back and front of the beam, respectively. In the model statement, the lift force, for simplicity, is situated at the body back section. m is the separation added mass at the back body section. A linearized solution of the problem (60) is determined using a quasi-rigid approximation for $(\mathbf{M}_*/\mathrm{Ei}_*)\to 0$. First order solution of Eq. (60) for $\mathrm{M}=\mathrm{const}$ is transformed to the system of more simple equations:

$$\text{a)}\ J\frac{d^2\eta}{dt^2}+k_\alpha amU_s^2\eta=0,$$

$$\text{b)}\ k_\alpha=\frac{1}{1+mU_s^2/K_b},\ \text{c)}\ K_b=\xi_b\frac{\mathrm{Ei}_m}{a^2}. \qquad (61)$$

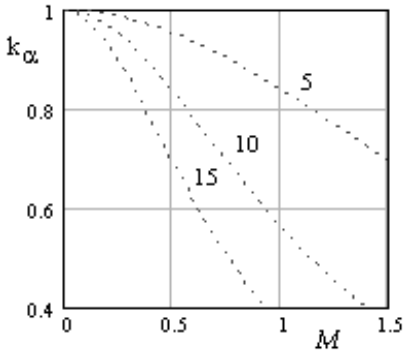

Figure 28: Hydro-elastic effects influence depend on M_∞

------- k_α Eq. (61b): bodies for aspect ratios $\lambda_b\sim 5,10,15$

Here, J is the longitudinal moment of inertia of the beam, i_m is the value of $i(x)$ at the center of mass, and the value of $\eta\approx\alpha$ (i.e., close to the angle of attack of the body at the center of mass). The solution for $\mathbf{M}=\mathrm{const}$ have been defined significance of $\xi_b\sim 4.8$ for this case. Physically hydro elastic effects are manifested here by more small attack angles in the back basis of body as compared to it's values for the rigid body.

Figure 28 illustrates the results of hydro-elastic effect action on attack angle at the back body section in case of model case of supercavitation flow of metallic body for $E\sim 4\times 10^{11}\,n/m^2$ of near parabolic form with essentially wetted back part of body. The estimation data for $k_\alpha=k_\alpha(M_\infty)$ on basis formulas (61b) depend on Mach Number are presented for three body aspect ratios $\lambda_b\sim 5,10,15$ and rough estimation of $\xi_b\sim 11.5$. With account of essential influence of real lift force position shift to forward this data can be preliminary oriented only.

6.4 Generalized system of the linearized equations with account of hydro-elasticity

These equations are on the basic model for nearly straight, inertial motion at nearly constant speed., The linearized model applies to very high-speed launching, with subsequent near straight body motion by inertia. The body has a wetted stabilizing part at the back, and the hydro-elastic effects are accounted for based on generalization of the model problem (60, 61). Neglecting small lateral forces on the disk-type cavitator and accounting for sufficiently slow damping of velocity, the system equation for the trajectory $\bar{y}=\bar{y}(\bar{x}),\ \bar{y}=y/a,\ x=x/a$ is defined as:

$$\text{a)}\ \frac{d^2\Delta\bar{y}}{d\bar{x}^2}+k_h\bar{m}\frac{d\Delta\bar{y}}{d\bar{x}}+k_h\frac{\bar{m}}{\bar{J}}\Delta\bar{y}=0,$$

$$\text{b)}\ \Delta\bar{y}\big|_{\bar{x}=0}=-\bar{J}(\alpha_o-\bar{J}\bar{\omega}_o),\ \left.\frac{d\Delta\bar{y}}{d\bar{x}}\right|_{\bar{x}=-\bar{J}\bar{\omega}_o}, \qquad (62)$$

$$\text{c)}\ \Delta\bar{y}=\bar{y}-\bar{J}(\alpha_o-\bar{J}\bar{\omega}_o)-(\theta_o+\bar{J}\bar{\omega}_o)\bar{x},$$

$$\text{d)}\ k_h=1/[1+\frac{mU_s^2}{K_h}],\ \frac{1}{K_h}=[\frac{1}{K_S}+\frac{1}{K_{b\Delta}}],\ K_{b\Delta}=\xi_{b\Delta}\frac{\mathrm{Ei}_m}{a^2}$$

Here, α_o, θ_o, U_o, ω_o, are the initial angle of attack, the angle tangential to the trajectory of the center of mass, linear velocity, and angular velocity, respectively. a is the distance between centers of mass and pressure. m is the separation-added mass of the back wetted part of the body, combined with any stabilizers interacting with cavity surfaces, **M**, **J** are the mass of the body and the longitudinal moment of inertia. E, i_m are the modulus of elasticity and lateral moment of inertia at the section of the center of mass, $K_{b\Delta}$ is the body rigidity (K_b - without influence of lift shift), defined in a special way, K_s is the stabilizer rigidity. For neglecting of the lateral forces on the disk cavitator delay effect for flow action on the back part of body in this model is not accounted. The problem (62) defines lateral trajectory coordinates relative to the axis inclined with respect to the direction of initial motion. The classical equation of harmonic oscillations (62a) with damping, can be expressed as equation depend any from values: α, θ, $(\alpha+\theta)$. Physically, this fact corresponds to lateral and angular oscillations of an elastic body, where energy

is transformed from one type of oscillation into another, with energy then transformed into lateral energy in the wake behind the body. It is important that this model is significantly unsteady, not quasi-steady. Even this simple linearized model for the case of a rigid body uncovers the most important properties of supercavitation motion connected with the manifestation of intensive oscillations, with definition of key parameters of this process. The amplitude A_{mp} and the frequency of the dying oscillations k_* are given by:

$$A_{mp} = e^{-\frac{k_h \bar{m}}{2} x} \sqrt{(\Delta \bar{y}_o)^2 + \frac{(\Delta \bar{y}_o^{\bullet} + 0.5 k_h \bar{m}\, \Delta \bar{y}_o)^2}{k_h \frac{\bar{m}}{\bar{J}} - (0.5 k_h \bar{m})^2}}, \qquad k_* = \sqrt{k_h \frac{\bar{m}}{\bar{J}} - (0.5 k_h \bar{m})^2}\ . \tag{63}$$

Oscillations frequency for M_∞, λ increasing have tendency to be more close to elastic body own frequencies of oscillations and indicate on possibility of resonance processes. This tendency can be enforced in transonic flow where possibility of essential increasing of lateral forces was discovered [37]. In doing so hydro-elastic effects action decreased lateral forces can provide considerable decreasing of these processes. The approach under consideration is essentially model approach so supposes linear dependence lateral forces on attack angle and is not taking into account cavity deformation along motion process. Nevertheless the simplest model of lateral motion can be considered as qualitative model applicable for estimations for wide enough cases. More precise approach is applied in [4].

CONCLUSIONS

A number of problems involving the launch of very high-speed supercavitating projectiles in water have been solved, but research overall remains incomplete at this time.

One of the remaining challenges is observed instability during repeated launch experiments, which appears to be associated with the very high stresses that occur during water entry. Special experiments are required to verify the underlying physics of this process.

Another important unfinished research topic is compressibility effects at high Mach number. This issue is important for defining reasonable expectations for the maximum launch speed that can be achieved in the attempts to increase range and avoid resonant regimes of motion. One promising approach would be the development and validation of nonlinear numerical models for compressible supercavitating flows past disk-type cavitators, which would allow for reliable predictions over a much greater range of Mach numbers.

Additional important results are desired in the area of experimental research into supercavitating flows and the motion of the projectile within the cavity at very high speeds and under very high pressure.

NOMENCLATURE

r, x, t	Cylindrical coordinates, time
$r = R(x,t)$	Axisymmetric cavity form
R_k, L_k, λ_k	Maximum radius, semi-length, aspect ratio of ordinary cavity for $\sigma = \text{const}$
$U_\infty,\ P_\infty, \rho_\infty$	Speed, pressure, mass density at infinity
$\sigma = \frac{\Delta P}{\rho_\infty U_\infty^2 / 2}$	Cavitation Number (ΔP -pressure difference hydrostatic and in cavity)
$M_\infty = U_\infty / a_\infty$	Mach Number (a_∞ -water sonic speed in undisturbed fluid)
$D\ ;\ c_{do}\ , c_d$	Drag, cavitator drag coefficients
C_{D0}, C_D	Cavitating drag coefficients per maximal cavity section for $\sigma = 0,\ \sigma > 0$

REFERENCES

[1] Mc-Millen J. H., Harwey E. N. A., 1946, "Spark Shadow graphic Study of Body Waves in Water," J. Appl. Phys., 17(7), pp. 541-555.

[2] Yakimov Yu. L., Yeroshin V.A., Romanenko No. I., 1978, Modeling of body motion with account of it's compressibility. "Some problems of Mechanics of continuous environment" MSU Press, Ruusia, pp. 29-23.

[3] Yakimov Yu L.,m1987, "Flows to limit of water", Mechanics and technical progress 2, NAUKA, pp. 7-25.

[4] Yeroshin V. A., 1991, "Penetration of elastic cylinder into water with high speed" - Preprint of Institute Mechanics of MSU - No. 5-91.

[5] Savchenko Yu. N., Semenenko V. N., Serebryakov V.V., 1993, "Experimental Research of Subsonic Cavitating Flows". J. DAN of Ukraine, 2, pp. 64-68. (Russ.)

[6] Vlasenko Yu., D., 2002, "Experimental investigations of supercavitation flows at subsonic and transonic velocities. Proc. of intern. conference: High Speed Hydrodynamics HSH 2002 – Cheboksary, Russia, pp. 197-204.

[7] Kirschner I., 1998, "Supercavitating Projectile Experiments at Supersonic Speeds", High-speed Body Motion in Water, Agard-R-827, pp. 35(1-4).

[8] Bivin Yu. K., Glukhov Yu. M., Permyakov Yu. V., 1985, "Vertical bodies water entry". J. Proc. of AS of USSR, series Fluid and Gas Mech., 6, pp.3-9. (Russ.)

[9] Woidneck Claus-P., 1986, "Rod penetration in liquids", Proc. of 9th international Symposium on ballistics -Part 2, pp. 392-445.

[10] Arndt R.E., 1998 "Cavitation" Handbook of Fluid Dynamics, Springer, 19, pp. 20(1 -13).

[11] Birkhoff G., Zarantonello E., 1957, "Jets, wakes and cavities". - New York: Academic Press.

[12] Gurevich M.I., 1978, "Theory of jets of ideal fluid", NAUKA, Moscow.

[13] Levinson N., 1946, "On the asymptotic shape of the cavity behind an axially nose moving through an ideal fluid", J. Annals of Mathematics. vol.47(.4). pp. 704-731.

[14] Logvinovich G. V., 1969, Hydrodynamics of Flows with Free Boundaries. - Kiev, NAUKOVA DUMKA.

[15] Gusevsky L. G., 1979, Numerical Analysis of Cavitation Flows, (Preprint of CO of AS USSR, Institute of Thermophysics, 40-79), Russia..

[16] Krasnov V. K., Kuznetsov V.K., 1989, "Application of method of boundary integral equations to the calculation

of two-dimensional and axisymmetric cavitating flows. " set: Actual Problems of Hydrodynamics, Cheboksary, Russia pp. 71-75.
[17] Kring D., Fine. N., Uhlman J., Kirschner I., "Unsteady cavitating model, using three-dimensional method of boundary elements." J. Applied Hydromechanics - 2000, 2(74), 3, pp. 53-59.
[18] Aleve G. A., 1983, "Separated flow of circular cone by transonic flow of water." J. Proc. of AS USSR, Fluid and Gas Mech. 2, pp.152-154 .
[19] Aleve G.A., 1984, "Separated flow over circular cone of finite length by supersonic flow of water. In set of papers: Dynamics of continuum with unsteady boundaries, Chuvashian Univerasity, Russia, pp.3-7.
[20] Terentiev A.G, Chechnev A.V., 1985, "Numerical Investigation of Plate and Disk Enter in Compressible Fluid," J. Proc. of AS USSR, Fluid and Gas Mech. 2, pp. 104-107.
[21] Vasin A.D., 1996, "Calculation of axisymmetric cavities behind disk in subsonic flow of compressible fluid", J. Proc. of AS USSR, Fluid and Gas Mech., .2, pp. 94-103.
[22] Zigangareieva L. M., Kiselev O. M., 1998, Subsonic Flow of Plate by Compressible Fluid under Small cavitation Numbers. J. Proc. of AS USSR, Fluid and Gas Mechanics -No. 4, pp. 94-104.
[23] Saurel R. Cocchi J.P., Butler P.B., 1999, Numerical study of cavitation in the wake of hypervelocity underwater projectile. J. Propulsion and Power. 15, (4), 513-523.
[24] Logvinovich G. V., Serebryakov V.V., 1975, "On methods of calculations of the form of slender axisymmetric cavities." J.Hydromechanics , 32, pp. 47-54.
[25] Petrov A. G., 1986, "Asymptotic expansions for slender axisymmetric cavities". J. ПМТФ, 5, pp. 45-49.
[26] Serebryakov V.V., 1973, "Asymptotic solution of the problem on slender axisymmetric cavity", J. DAN of Ukraine SSR, ser. A, 12, pp.1119 - 1122.
[27] Serebryakov V. V., 1981, "Calculation of slender axisymmetric cavity forms in unsteady flow for a number of characteristic cases. J. Hydromechanics, 44, pp. 86-94.
[28] Serebryakov V. V.", 1992, "Asymptotic Solutions of Axisymmetric Problems for Sub- and Supersonic Separated Flows for Zero Cavitation Numbers". J. DAN of Ukraine , 9, pp.66-71. (Russ.)
[29] Serebryakov V.V., 1994, "Asymptotic Solutions of the Flows with Developed Cavitation on the Basis of Slender Body Approximation" J. Hydromechanics, 68, pp. 62-74.
[30] Serebryakov V.V., 2002, Models of the Supercavitation Prediction for High-Speed Motion in Water. Proc. of intern. Conference "High-speed Hydrodynamics": HSH-2002, Cheboksary, Russia, pp.71-92.
[31] Serebryakov. V, Schnerr G., 2003, "Some Problems of Hydrodynamics for Sub- and Supersonic Motion in Water with Supercavitation. Proc. of CAV2003: Osaka, Japan.
[32] Serebryakov V. V., 2007, Compressibility effects for very high sub-, trans- and supersonic speeds of motion in water. Proc. of APM2007, St. Petersburg, pp.378-390.
[33] Varghese A., Uhlman J., Kirschner I., 1997, "Axisymmetric slender-body analysis of supercavitation high-speed bodies in subsonic flow," Proc. of conference in RI - pp. 185-200.
[34] Sagomonian A.Y., 1974, Penetration, MSU Univ., Russia.
[35] Paryshev E. V., 2002, "The plane problem of immersion of an expanding cylinder trough a cylindrical free surface of variable radius. Proc. of intern. conference High-speed Hydrodynamics: HSH2002 -, Cheboksary, pp. 277-285.
[36] Fine N. E., Uhlman J. S., 2002, 'Calculation of the added mass and damping forces on supercavitating bodies,' Proc. of the Intern. Conference High-speed Hydrodynamics-HSH-2002, Cheboksary, pp. 127-138.
[37] Mayboroda A. N., 2002, 'Gliding for sub- and supersonic speeds,' Proc. of intern. Conference: High-speed Hydrodynamics: HSH2002, Cheboksary, Russia.
[38] Kubenko V.D., 2003, Not steady lateral motion of slender long body under supercavitation flow. J. DAN of Ukraine, 6, pp. 41-48.
[39] Filippov V.I., 1987, "Compressibility influence on sizes of cavities", Interactions of bodies in fluid with free boundaries, Chuvashian Univ., Russia, pp. 115-122.
[40] Kuznetsov A.., Manevich A., 1979, "Vertical enter of inclined slender symmetric profile into compressible fluid." J. Proc. of AS USSR,Fluid and Gas Mech. 5.
[41] Nishiyama T. and Khan O., 1981, Compressibility effects upon cavitation in high-speed liquid flow (Transonic and supersonic liquid flows). "Bulletin of the Japanese Society of Mechanical Engineers - 24, 190.
[42] Schnerr, G.H., Schmidt, S.J., Sezal, I.H., Thalhamer, M., 2006, Shock and Wave Dynamics in Compressible Liquid Flows with Emphasis on Unsteady Load on Hydrofoils and on Cavitation in Injection Nozzles, Invited Lecture. Proc. CAV2006 - 6th Int. Symposium on Cavitation, Wageningen, The Netherlands, CD-ROM publication.
[43] Gieseke T., 2001, Optimization of Supercavitating Projectile Performance. Proc. of Forth Int. Symposium on Cavitation: CAV2001, Pasadena, USA.
[44] Kirschner, I.N., Rosenthal, B.J., Uhlman, J.S., 2003 Simplified Dynamical Systems Analysis of Supercavitating High-Speed Bodies, Proc. of Fifth International Symposium on Cavitation - CAV 2003, Osaka, Japan.
[45] Epshteyn L. A., Lapin V.M., 1980, "Approximate calculation of boundaries influence on cavity length in plane problem and behind axisymmetric body", J. Proceedings of CAHI, 2060, pp. 3-24.
[46] Nesteruk I.G, Semenenko V.N, 2006 " Problems supercavitating motion range by inertia optimization with fixed end depth", J. Applied Hydromechanics 8(4), pp. 33-42.